

University of Nebraska - Lincoln

DigitalCommons@University of Nebraska - Lincoln

---

HPRCC Personnel Publications

High Plains Regional Climate Center

---

4-2020

## A Hydrometeorological Assessment of the Historic 2019 Flood of Nebraska, Iowa, and South Dakota

Paul Flanagan

Rezaul Mahmood

Natalie Umphlett

Erin M.K. Haacker

Chittaranjan Ray

*See next page for additional authors*

Follow this and additional works at: <https://digitalcommons.unl.edu/hprccpubs>



Part of the [Atmospheric Sciences Commons](#), [Climate Commons](#), [Environmental Indicators and Impact Assessment Commons](#), [Environmental Monitoring Commons](#), [Fresh Water Studies Commons](#), [Hydrology Commons](#), [Meteorology Commons](#), [Natural Resources Management and Policy Commons](#), [Sustainability Commons](#), and the [Water Resource Management Commons](#)

---

This Article is brought to you for free and open access by the High Plains Regional Climate Center at DigitalCommons@University of Nebraska - Lincoln. It has been accepted for inclusion in HPRCC Personnel Publications by an authorized administrator of DigitalCommons@University of Nebraska - Lincoln.

---

**Authors**

Paul Flanagan, Rezaul Mahmood, Natalie Umphlett, Erin M.K. Haacker, Chittaranjan Ray, Bill Sorensen, Martha Shulski, Crystal J. Stiles, David Pearson, and Paul Fajman

---



1 **A Hydrometeorological Assessment of the Historic 2019 Flood of Nebraska, Iowa,**  
2 **and South Dakota**

3  
4 Authors:

5 Paul Xavier Flanagan<sup>1,2</sup>, Rezaul Mahmood<sup>1,2</sup>, Natalie A. Umphlett<sup>1,2</sup>, Erin Haacker<sup>3</sup>, C.  
6 Ray<sup>4</sup>, William Sorensen<sup>1,2</sup>, Martha Shulski<sup>2,5</sup>, Crystal J. Stiles<sup>1,2</sup>, David Pearson<sup>6</sup>, Paul  
7 Fajman<sup>6</sup>

8  
9 Affiliations:

10 <sup>1</sup>High Plains Regional Climate Center, University of Nebraska-Lincoln, Lincoln,  
11 Nebraska, USA

12 <sup>2</sup>School of Natural Resources, University of Nebraska-Lincoln, Lincoln, Nebraska, USA

13 <sup>3</sup>Department of Earth and Atmospheric Sciences, University of Nebraska-Lincoln,  
14 Lincoln, Nebraska, USA

15 <sup>4</sup>Nebraska Water Center, University of Nebraska-Lincoln, Lincoln, Nebraska, USA

16 <sup>5</sup>Nebraska State Climate Office, University of Nebraska-Lincoln, Lincoln, Nebraska,  
17 USA

18 <sup>6</sup>The National Weather Service, Omaha, Nebraska, USA

19

20 *Corresponding author address:* Paul Flanagan, High Plains Regional Climate Center,  
21 School of Natural Resources, 701 Hardin Hall South, 3310 Holdrege Street, Lincoln, NE,  
22 68583. Email: pflanagan3@unl.edu; Phone: 402-472-6706

**Early Online Release:** This preliminary version has been accepted for publication in *Bulletin of the American Meteorological Society*, may be fully cited, and has been assigned DOI 10.1175/BAMS-D-19-0101.1. The final typeset copyedited article will replace the EOR at the above DOI when it is published.

23 **Abstract**

24           During early 2019, a series of events set the stage for devastating floods in eastern  
25 Nebraska, western Iowa, and southeastern South Dakota. When the floodwaters hit, dams  
26 and levees failed, cutting off towns, while destroying roads, bridges, and rail lines, further  
27 exacerbating the crisis. Lives were lost and thousands of cattle were stranded. Estimates  
28 indicate that the cost of the flooding has topped \$3 billion as of August 2019, with this  
29 number expected to rise.

30           After a warm and wet start to winter, eastern Nebraska, western Iowa, and  
31 southeastern South Dakota endured anomalously low temperatures and record-breaking  
32 snowfall. By March 2019, rivers were frozen, frost depths were 60-90 cm, and the water  
33 equivalent of the snowpack was 30-100 mm. With these conditions in place, a record-  
34 breaking surface cyclone rapidly developed in Colorado and propagated eastward,  
35 producing heavy rain towards the east and blizzard conditions toward the west. In areas of  
36 eastern Nebraska, western Iowa, and southeastern South Dakota, rapid melting of the  
37 snowpack due to this rain-on-snow event quickly led to excessive runoff that overwhelmed  
38 rivers and streams. These conditions brought the region to a standstill.

39           In this paper, we will provide an analysis of the antecedent conditions in eastern  
40 Nebraska, western Iowa and southeastern South Dakota, the development of the surface  
41 cyclone that triggered the historic flooding, along with a look into the forecast and  
42 communication of flood impacts prior to the flood. The study used multiple datasets,  
43 including in-situ observations and reanalysis data. Understanding the events that led to the  
44 flooding could aid in future forecasting efforts.

45 **Introduction**

46 During the late winter season of 2019, a combination of anomalous events led to  
47 devastating floods across the central United States (U.S.; Fig. 1). These events were  
48 punctuated by the passage of an extraordinarily deep surface cyclone that propagated  
49 across the region on 12-14 March. This storm system produced extreme weather, including  
50 blizzard conditions stretching from Colorado and Kansas through the Dakotas, and  
51 widespread liquid precipitation events in areas just to the east. Numerous daily  
52 precipitation records were broken, with some locations setting new records for highest one-  
53 day precipitation for the month of March. Low pressure records over Colorado and Kansas  
54 were also broken. This flood event was exacerbated by the surface conditions across  
55 eastern Nebraska, western Iowa, and southeastern South Dakota (hereafter referred to as  
56 the study area), namely the widespread frozen or saturated soils, frozen rivers, and above  
57 average river streamflow conditions (Fig. 2a) that led to numerous record river crests across  
58 the region (Fig. 2b, 2c, 2d, 9c). Initially, the excessive runoff overwhelmed smaller  
59 tributary rivers in study area, which flow to larger rivers in the Platte and Missouri River  
60 basins. This resulted in failed levees and dams, leaving downriver locations overwhelmed  
61 with significant ice jams and water flow. This set of circumstances led to one of the most  
62 catastrophic flood events documented across the study area. Prior to the event, National  
63 Weather Service (NWS) offices were forecasting and communicating the possibility of  
64 record-breaking floods across the study area. Ultimately, the Federal Emergency  
65 Management Agency (FEMA) declared a major disaster for both Nebraska and Iowa, with  
66 a preliminary damage estimate of at least \$3 billion.

67 No single factor can explain the occurrence of this historic flood event. Hence, it  
68 is critical to understand how the combination of meteorological, climatological, and  
69 hydrological conditions led to large-scale flooding across the region. The purpose of this  
70 brief paper is to 1) discuss the rapid cyclogenesis event and preceding surface and  
71 hydrological conditions across eastern Nebraska, western Iowa, and southeastern South  
72 Dakota, 2) examine how the synergy between these independent factors led to large-scale  
73 major flooding, and 3) investigate the forecast and communication of flood impacts across  
74 Nebraska, Iowa, and South Dakota.

75

## 76 **Prior Hydrometeorological Context**

77 During the 2018 fall (Fig. 3a) and 2018/2019 winter (Fig. 3b) seasons, sea surface  
78 temperatures (SST) across the tropical Pacific were warmer than normal, (Fig. 3) indicating  
79 a developing El Niño event. These SST conditions increased the chances of a wetter winter  
80 season across the southern U.S., near normal moisture conditions in the study area, and a  
81 milder winter season across the northern U.S., including most of the study area (Climate  
82 Prediction Center 2017). Additionally, the North Atlantic Oscillation (NAO) was positive  
83 during December and January (0.61 and 0.59), the Arctic Oscillation (AO) was weakly  
84 positive (December; 0.110) and negative (January; -0.713), and the Pacific-North  
85 American (PNA) teleconnection pattern was positive (0.86 and 0.83) (available at  
86 <https://www.cpc.ncep.noaa.gov/products/precip/CWlink/pna/nao.shtml>,  
87 [https://www.cpc.ncep.noaa.gov/products/precip/CWlink/daily\\_ao\\_index/ao.shtml](https://www.cpc.ncep.noaa.gov/products/precip/CWlink/daily_ao_index/ao.shtml), and  
88 [https://www.cpc.ncep.noaa.gov/products/precip/CWlink/pna/norm.pna.monthly.b5001.cu  
89 rrent.ascii.table](https://www.cpc.ncep.noaa.gov/products/precip/CWlink/pna/norm.pna.monthly.b5001.curent.ascii.table), respectively). It is well known that the positive NAO would force slightly

90 warmer temperatures over the central U.S. with little impact on precipitation (Hurrell et al.  
91 2003), the weak AO would not largely impact the overall weather (Wang et al. 2005), and  
92 the positive PNA would drive warmer temperatures over the western and north central U.S.  
93 (Leathers et al. 1991). The early part of the winter season (December 2018 and January  
94 2019) was warmer and wetter relative to February and March in the study area (Fig. 4).  
95 Runoff from river systems were above average across most of the region (Fig. 2a) prior to  
96 freezing. Precipitation across the region was above normal (Fig. 4c), with average snowfall  
97 totals through the end of January at approximately 30.5 cm. Even so, because of the warmer  
98 early winter season temperatures (Fig. 4a), no significant snowpack had developed by the  
99 end of January. Part of the moisture from the early winter season precipitation (either rain  
100 or snow) was absorbed by the land surface and as a result, soils were nearly saturated during  
101 this portion of 2019 (Fig. 2e). In January, temperatures across the study area had begun to  
102 decrease such that the soils were frozen by the end of the month.

103         It was also found that the center of the warm SST anomalies in the Pacific had  
104 shifted from the early to late winter. The primary center was now seen in the central tropical  
105 Pacific (Fig. 3b). This location of warm SST anomalies has been linked to increased  
106 chances of excessive precipitation over the south-central U.S. (Livezey et al. 1997;  
107 Flanagan et al. 2019). Further, these central Pacific warm SST anomalies are not associated  
108 with the typical higher chance of northern U.S. warming, seen during typical eastern  
109 tropical Pacific warm events (Ashok et al. 2007). The NAO continued to be positive during  
110 February and March (0.29 and 1.23), the AO became strongly positive (1.149 and 2.116),  
111 and the PNA shifted to negative (-1.08 and 0.25), with the month of March showing a  
112 positive PNA index owing to large (~ 0.5 to 1.3) positive daily PNA values after the

113 cyclogenesis event. This is an interesting feature, as both positive NAO and AO would  
114 normally aid in keeping temperatures milder during the winter season over the central U.S.  
115 As indicated above, this was not the case. The colder temperatures during February and  
116 March were caused by a persistent northwesterly flow regime over the northwestern and  
117 north central U.S. due to ridging across the northwestern U.S. The negative PNA regime  
118 can force such a pattern over this portion of the U.S. (Leathers et al. 1991). Thus, the cold  
119 temperatures were linked to the persistent negative PNA signal during this portion of winter  
120 2019. Frigid temperatures occurred across the region from late January through March  
121 (Fig. 4b). This shift in temperatures finally caused rivers to freeze, with the Platte River  
122 having an ice depth around 43 cm (at Leshara, Nebraska). Further, with wet soils and  
123 lacking an insulating snowpack, the cold temperatures formed a deep and hard frost layer  
124 prior to March (Fig. 5a). With these cooler temperatures came a changeover of  
125 precipitation, as snowfall began to occur more frequently. The above average precipitation  
126 resulted in numerous snowfall records being broken across the region (Fig. 4c, 4d), setting  
127 up a deep and moist snowpack (Fig. 5b, 5d). Approximately 10-20 cm of snow was  
128 observed across the region (Fig 5b), with the snowpack showing around 3-10 cm of snow  
129 water equivalent (SWE) (Fig. 5d). The frozen soil did not allow for infiltration of moisture  
130 from melted snow and expected that a rapid melting would spell disaster for the region.

131         The Global Historical Climatology Network stations that show the season's top-5  
132 snowfall records for 2018-2019 are highlighted in figures 4c and 4d. It is to be noted that  
133 other stations within the region had 'records' but did not pass the quality control checks  
134 we utilized to produce the station plots. In previous spring flood events, namely 1881 and  
135 1952, hydrometeorological conditions were similar to conditions of 2019. For the 1881



136 floods, 60-80 cm of river ice was reported and for the 1952 event, SWE values were around  
137 8-13 cm along with saturated soils from wetter than average fall and winter seasons  
138 (Department of Commerce, Hydrologic Services Division 1954). Overall, the region was  
139 setup for a flood near or above the previous floods of record in the region. Early winter  
140 hydrological conditions, extreme cold and anomalous precipitation during the later winter  
141 put in place conditions ready for a rapid, significant flood event for the study region.

142

### 143 **Rapid Cyclogenesis of March 12-14, 2019**

144 Reanalysis data from the National Centers for Environmental Prediction/National  
145 Center for Atmospheric Research (NCEP/NCAR) Reanalysis version 1 (Kalnay et al.  
146 1996) were utilized to provide a synoptic overview of the event. The dataset is available  
147 from the Earth System Research Laboratory (ESRL) Physical Science Division (PSD)  
148 database (<https://www.esrl.noaa.gov/psd/data/gridded>). This 2.5° x 2.5° globally gridded  
149 dataset is updated daily, from 1948 to present. Using this dataset, we analyzed sea level  
150 pressure (SLP); surface temperature and winds; precipitable water; 250 and 500 hPa winds  
151 and geopotential heights; and 850 and 925 hPa winds, temperature, and heights using the  
152 NCAR Command Language (NCL; <http://dx.doi.org/10.5065/D6WD3XH5>). This dataset  
153 was utilized to derive all advection terms. Standardized anomalies were created for  
154 temperature, geopotential height, precipitable water, and SLP to present critical variables  
155 in the context of the time of year and regional climate. This was accomplished by using  
156 21-day centered means from a 30-year base period (1981-2010) and standardized by the  
157 standard deviation, given by

158 
$$\sigma_A = \frac{X - \mu}{\sigma}$$

159 where  $X$  is the observed grid-point value,  $\mu$  is the centered 21-day climatological mean,  
160 and  $\sigma$  is the standard deviation (Durkee et al. 2012).

161 On 12-13 March, a rapid surface cyclogenesis event took place across the central  
162 U.S. (Fig. 6). A closed trough across the southwestern U.S. propagated towards the north  
163 at the same time as a long-wave trough shifted down from the north. These two systems  
164 began interacting late on 12 March, in the lee of the Rocky Mountains in eastern Colorado.  
165 As this area already had a low-pressure zone near the surface (Fig. 6a), and owing to the  
166 converging troughs across the region (Fig. 6c, 6d), a rapid lee cyclogenesis event took place  
167 (Fig. 6b). This caused surface pressure values to plummet, leading to a record-low pressure  
168 reading over eastern Colorado (970.4 hPa; NWS Cheyenne WY 2019; Colorado Climate  
169 Center 2019) and Kansas (974.7 mb; NWS Dodge City, KS 2019), with a drop of 24 hPa  
170 (from 994 hPa to 970 hPa) in 15 hours on 12 March (NWS Hastings NE 2019). This rapid  
171 lee cyclogenesis event was the primary driver of the excessive precipitation which occurred  
172 over the study region on 13 March.

173 However, prior to this cyclogenesis event, the gradient zone between the upper  
174 level closed trough and the broad ridge over the eastern U.S. (Fig. 6c) caused southerly  
175 flow across a majority of the central U.S. (Fig. 7a). This caused warm, moist air to begin  
176 to advect over the central part of the country (Fig. 7b). As the cyclogenesis event began to  
177 take place, the advection regime strengthened, bringing an anomalously warm (Fig. 7c)  
178 and near record breaking deep moist airmass over the central U.S. (Fig. 7d). This is  
179 reflected in the record precipitable water values across the region, with atmospheric

180 soundings at Omaha, NE (2.44 cm) and North Platte, NE (1.80 cm) breaking their 13 March  
181 0000 UTC records (2.159 and 1.37 cm, respectively) and Topeka, KS (2.57 cm) nearly  
182 breaking its record (2.62 cm) at 12 March 1200 UTC. Note that all of these soundings were  
183 taken prior to precipitation in their area. The advection of warm air resulted in rapid snow  
184 melt that reduced the snowpack from a peak depth of 10-30 cm on 9 March to a trace on  
185 15 March across most of eastern Nebraska and western Iowa (Fig. 5b, 5c). While  
186 temperatures were not high enough to cause large scale snowmelt in southeastern South  
187 Dakota (Fig. 5b, 5c), temperatures were warm enough for the precipitation to fall as rain  
188 instead of snow (NWS Sioux Falls SD 2019). This can further be seen in the SWE figures  
189 (Fig. 5d, 5e), which show a rapid decrease across most of Nebraska and Iowa, while only  
190 extreme southeastern South Dakota saw a large decrease in snow coverage and the  
191 remainder of South Dakota maintained its snowpack. Thus, when rainfall began later on  
192 12 March, runoff from prior snowmelt was already flowing into the region's streams and  
193 rivers. The excessive precipitation forced by the cyclone quickly caused rivers to rise to  
194 record-setting levels, overwhelming regional water storage infrastructure (Fig. 2b).

195

## 196 **Flood Forecast Discussion**

197 Prior to the event, the Weather Prediction Center (WPC) forecasting approximately  
198 50-75 mm in their 72-hour Quantitative Precipitation Forecast (QPF) from 0000 UTC 12  
199 March to 0000 UTC 15 March (Fig. 8). The system was expected to efficiently produce  
200 precipitation from the anomalously moist air mass that was being advected into the area as  
201 the lee cyclone rapidly developed and propagated to the northeast.

202           Weeks prior to the flooding event, NWS Omaha/Valley officials were in  
203 communication with regional officials (emergency managers, Nebraska Emergency  
204 Management Agency (NEMA), etc.) and local media regarding the risk of flooding because  
205 of the extensive ice coverage of regional rivers. There were weekly ice jam update  
206 conference calls with core NWS Omaha/Valley partners and local media. The latter relayed  
207 flood potential and rainfall forecast information to stakeholders and local and state officials  
208 in the weeks leading up to the flood event. These conference calls disseminated the  
209 probabilistic risk of spring flood events, using information such as current streamflow  
210 percentiles, river ice status, snowpack depth, etc. As 12 March drew closer, clarity into the  
211 extreme nature of the event increased. A week prior to the flood event, NWS Omaha/Valley  
212 sent out an updated spring flood outlook, which highlighted an increased threat for major  
213 flooding owing to the anomalous hydrological conditions throughout the area. When the  
214 model output precipitation forecast for 12 March to 14 March started to take focus, local  
215 NWS offices began issuing flood watches for the region. Subsequently, these watches were  
216 updated to reflect the expected record-breaking nature of the event on the morning of 12  
217 March over a large section of the NWS Omaha/Valley forecast area. These forecasts were  
218 supported by numerous observational (e.g., streamflow, river ice and snowpack) and  
219 modeling resources (e.g., GEFS, ECMWF) including the ensemble situational awareness  
220 table (ESAT) which showed the potential for an extreme event a week prior to the flood  
221 event.

222           The first round of precipitation came in the late afternoon on 12 March, but did not  
223 produce large-scale precipitation across the region as the forcing for ascent was weak at  
224 this time. Later, on 12-13 March, multiple rounds of precipitation came through the study

225 area, as forecasted. Most areas in eastern Nebraska and western Iowa received around 12-  
226 25 mm of liquid precipitation with isolated areas reporting around 25-50 mm (Fig. 9a).  
227 However, areas farther west, mainly in the tributary region of the Platte River (e.g. the  
228 Loup and Wood Rivers) and in southeastern South Dakota, received 40-75 mm of primarily  
229 liquid precipitation on 12-14 March. Thus, the storm total precipitation amounts matched  
230 well with the WPC forecasted precipitation totals. At approximately 1400 UTC 14 March,  
231 precipitation began to cease in the study region due to a rapidly developing area of dry air  
232 forced by the occlusion process of the surface low. Farther west in Nebraska and South  
233 Dakota, snowfall began or continued to fall on the cold side of the occluding cyclone,  
234 causing blizzard conditions and producing around 15 cm of snow across most of the  
235 western portions of Nebraska and South Dakota (Fig. 9b). This snow would later melt and  
236 further exacerbate flood conditions across the region. Due to the existing snowpack and  
237 frozen soil conditions, almost all of this precipitation quickly ran into rivers and creeks.  
238 The large amount of water produced by the melting snow (Fig. 9c) and the excessive runoff  
239 from the liquid precipitation quickly overwhelmed the watersheds across the region and  
240 verified the NWS flood warnings.

241

## 242 **Summary and Perspective**

243 During mid-March of 2019, the study area was impacted by record-setting floods.  
244 This flood event was triggered by precipitation forced by the record-low surface cyclone  
245 that rapidly developed across eastern Colorado and brought record daily precipitation  
246 amounts across portions of Nebraska, either through rain or the heavy snowfall. Preceding  
247 the flood event, weeks of anomalously low surface temperatures and accumulation of snow

248 prior to the cyclogenesis event caused soil conditions that led to anomalously high runoff.  
249 In addition, warm advection and rainfall quickly melted the abnormally thick snowpack  
250 that blanketed most of the study region. Although the rapid cyclogenesis of the lee cyclone  
251 in eastern Colorado is typical for this time of the year (Petterssen 1956; Chung et al. 1976;  
252 Roebber 1984; Pierrehumbert 1986; Clark 1990; Schultz and Doswell 2000), this particular  
253 event produced a surface cyclone that was more intense than any previously recorded in  
254 the Colorado and Kansas. Together, the record deep low-pressure system and the  
255 anomalously moist air mass brought about 12-25 mm of precipitation over southeastern  
256 Nebraska and southwestern Iowa, 25-50 mm across northeastern Nebraska and  
257 northwestern Iowa, and 40-75 mm over large portions of central Nebraska and southern  
258 South Dakota. With the rapidly melting, moist snow pack and ice jams on the waterways,  
259 the precipitation quickly exceeded the channel flow capacity of rivers in the region and  
260 began the expansive flooding.

261 While not a focus of the research presented here, the authors believe the extensive  
262 and costly event highlights the current forecasting ability of the WPC QPF capabilities.  
263 Their forecasts weeks and days ahead of the primary and catastrophic flood event across  
264 the study region provided much-needed warning far enough ahead of time that it likely  
265 saved numerous lives and personal property. This was aided by the probabilistic and  
266 deterministic forecasts which showed the heightened risk for an extreme weather event and  
267 subsequent flood a week before the cyclogenesis event occurred. Further, this successful  
268 forecast highlights the importance of extensive, high spatial resolution monitoring  
269 networks. Without the knowledge of the frozen soils and large snowpack across the region,  
270 local NWS offices would have lacked crucial information into the scale and magnitude of

271 the flood event that took place. Further, this event established far above normal  
272 hydrological conditions throughout the study region, i.e., the Missouri River Basin. After  
273 the flood event in March, meteorological and hydrological conditions have been such that  
274 the region is still completely saturated heading into the 2019-2020 winter season, meaning  
275 that river levels are largely above normal and soil moisture levels are at or near capacity.  
276 Further, owing to the above average water conditions throughout the Missouri River Basin,  
277 heavy precipitation events throughout 2019 caused rapid flood events, especially in  
278 southeastern South Dakota. It would be remiss not to note that the flood event of March  
279 2019 helped to developed extreme hydrologic conditions across Nebraska, Iowa and South  
280 Dakota which are conducive for further flood events in 2020. Lastly, this event underscored  
281 the importance of communication between forecasters and local/regional stakeholders,  
282 local officials and the media. This allowed NWS officials to disseminate crucial flood  
283 forecast information to “key players” rather than using the time prior to the event searching  
284 for “the right people to talk to.”

285

## 286 **Acknowledgements**

287 NCEP/NCAR reanalysis data was taken from the NOAA-ESRL Physical Sciences  
288 Division, Boulder Colorado from their Web site at  
289 <https://www.esrl.noaa.gov/psd/data/gridded>. CPC Global Unified Precipitation data  
290 provided by the NOAA/OAR/ESRL PSD, Boulder, Colorado, USA, from their Web site at  
291 <https://www.esrl.noaa.gov/psd/>. We would like to thank NCAR for the NCAR Command  
292 Language (Version 6.2.1) [Software]. (2014). Boulder, Colorado:  
293 UCAR/NCAR/CISL/TDD. <http://dx.doi.org/10.5065/D6WD3XH>.

294

295 **References**

296 American Meteorological Society, 2019: Lee Cyclogenesis. Accessed 29 July 2019,  
297 [http://glossary.ametsoc.org/wiki/Lee\\_cyclogenesis](http://glossary.ametsoc.org/wiki/Lee_cyclogenesis)

298 American Meteorological Society, cited 2019: "Lee Cyclogenesis". Glossary of  
299 Meteorology. [Available online  
300 at [http://glossary.ametsoc.org/wiki/Lee\\_cyclogenesis](http://glossary.ametsoc.org/wiki/Lee_cyclogenesis)]

301 Ashok, K., S. K. Behera, S. A. Rao, H. Weng, and T. Yamagata, 2007: El Niño Modoki  
302 and its possible teleconnection. *J. Geophys. Res.*, **112**, C11007.  
303 doi:10.1029/2006JC003798.

304 Chung, Y-S, K. D. Hage and E. R. Reinelt, 1976: On lee cyclogenesis and airflow in the  
305 Canadian Rocky Mountains and the East Asian mountains, *Mon. Wea. Rev.*, **104**,  
306 879–891.

307 Clark, J. H. E., 1990: An observational and theoretical study of Colorado lee  
308 cyclogenesis. *J. Atmos. Sci.*, **47**,1541–1561.

309 Colorado Climate Center, 2019: Storm Records. Accessed 9 December 2019,  
310 [https://climate.colostate.edu/pdfs/storm\\_records.pdf](https://climate.colostate.edu/pdfs/storm_records.pdf)

311 CPC, 2017: El Niño and La Niña – related winter features over North America. Accessed  
312 22 August 2019,  
313 [https://www.cpc.ncep.noaa.gov/products/analysis\\_monitoring/ensocycle/nawinter](https://www.cpc.ncep.noaa.gov/products/analysis_monitoring/ensocycle/nawinter)  
314 .shtml



315 Department of Commerce, Hydrologic Services Division, 1954: Floods of 1952 Upper  
316 Mississippi – Missouri – Red River of the North. *Technical Report 23*, 101 pp,  
317 [https://www.nws.noaa.gov/oh/hdsc/Technical\\_papers/TP23.pdf](https://www.nws.noaa.gov/oh/hdsc/Technical_papers/TP23.pdf)

318 Durkee, J. D., L. Campbell, K. Berry, D. Jordan, G. Goodrich, R. Mahmood,  
319 and S. Foster, 2012: A synoptic perspective of the record 1–2 May 2010 mid-South  
320 heavy precipitation event. *Bull. Amer. Meteor. Soc.*, **93**, 611–620.

321 Flanagan, P. X., J. B. Basara, J. C. Furtado, E. R. Martin, X. Xiao, 2019: Role of sea surface  
322 temperatures in forcing circulation anomalies driving United States Great Plains  
323 pluvial years. *J. Climate*, EOR, doi: <https://doi.org/10.1175/JCLI-D-18-0726.1>

324 Hurrell, J. W., Y. Kushnir, G. Ottersen, and M. Visbeck, 2003: *The North Atlantic*  
325 *Oscillation: Climate Significance and Environmental Impact*. *Geophys.*  
326 *Monogr.*, Vol. 134, Amer. Geophys. Union, 279 pp.

327 Kalnay, E., and Coauthors, 1996: The NCEP/NCAR 40-Year Reanalysis Project. *Bull.*  
328 *Amer. Meteor. Soc.*, **77**, 437–471.

329 Leathers, D. J., B. Yarnal, and M. A. Palecki, 1991: The Pacific/North American  
330 teleconnection pattern and United States climate. Part I: Regional temperature and  
331 precipitation associations. *J. Climate*, **4**, 517–528.

332 Livezey, R. E., M. Masutani, A. Leetmaa, H. Rui, M. Ji, and A. Kumar, 1997: 882  
333 Teleconnective response of the Pacific–North American region atmosphere to 883  
334 large central equatorial Pacific SST anomalies. *J. Climate*, **10**, 1787–1820, 884  
335 [https://doi.org/10.1175/1520-0442\(1997\)0102.0.CO;2](https://doi.org/10.1175/1520-0442(1997)0102.0.CO;2).

336 Nebraska Emergency Management Agency, 2019: News release, By the numbers –  
337 Nebraska’s historic floods.  
338 <https://nema.nebraska.gov/sites/nema.nebraska.gov/files/press/doc/NEMA%20A>  
339 [M%20NewRelease%203.17.19.pdf](https://nema.nebraska.gov/sites/nema.nebraska.gov/files/press/doc/NEMA%20A).

340 National Weather Service Cheyenne, Wyoming Office, 2019: March 13<sup>th</sup> and 14<sup>th</sup>, 2019  
341 Bomb Blizzard, Accessed 29 July 2019,  
342 <https://www.weather.gov/cys/March13142019Blizzard>

343 National Weather Service Hastings, Nebraska Office, 2019: Mid-March 2019: Historical,  
344 Catastrophic Flooding Impacts Parts of Central/South Central Nebraska, Accessed  
345 29 July 2019, <https://www.weather.gov/gid/march2019flood>

346 National Weather Service Sioux Falls, South Dakota Office, 2019: Heavy Rain and Snow  
347 Melt Create Widespread Flooding – March 13-14, 2019, Accessed 15 November  
348 2019, <https://www.weather.gov/fsd/20190314-Flooding>

349 National Weather Service Dodge City, Kansas Office, 2019: Historic low pressure system  
350 affects the Plains!, Accessed 9 December 2019,  
351 [https://www.weather.gov/ict/event\\_20190313](https://www.weather.gov/ict/event_20190313)

352 Petterssen, S., 1956: *Weather Analysis and Forecasting. Volume I: Motion and Motion*  
353 *Systems*. McGraw-Hill, 428 pp.

354 Pierrehumbert, R. T., 1986: Lee cyclogenesis. *Mesoscale Meteorology and Forecasting*, P.  
355 S. Ray, Ed., Amer. Meteor. Soc., 493–515.

356 Roebber, P. J., 1984: Statistical analysis and updated climatology of explosive cyclones,  
357 *Mon. Wea. Rev.*, **112**, 1577–1589.

358 Schultz, D. M., and C. A. Doswell III, 2000: Analyzing and forecasting Rocky Mountain  
359 lee cyclogenesis often associated with strong winds. *Wea. Forecasting*, **15**, 152–  
360 173.

361 Wang, D., C. Wang, X. Yang, and J. Lu, 2005: Winter Northern Hemisphere surface air  
362 temperature variability associated with the Arctic Oscillation and North Atlantic  
363 Oscillation. *J. Geophys. Res. Lett.*, **32**, L16706,  
364 doi:<https://doi.org/10.1029/2005GL022952>.

365

## Figure Captions

366

367 Figure 1: European Space Agency (ESA) (a) Sentinel-2A Level-1C visible band satellite  
368 image on 16 March 2019. Panel (b) Sentinel-2A Level-1C visible band satellite image on  
369 10 January 2019. Also included is a zoomed-out image from 16 March 2019 showing the  
370 location of the zoomed in area for (a) and (b). Sentinel-2 images taken from  
371 [https://apps.sentinel-hub.com/eo-browser/?lat=40.2685&lng=-](https://apps.sentinel-hub.com/eo-browser/?lat=40.2685&lng=-95.6738&zoom=10&time=2019-03-16&preset=1_TRUE_COLOR&datasource=Sentinel-2%20L2A)  
372 [95.6738&zoom=10&time=2019-03-](https://apps.sentinel-hub.com/eo-browser/?lat=40.2685&lng=-95.6738&zoom=10&time=2019-03-16&preset=1_TRUE_COLOR&datasource=Sentinel-2%20L2A)  
373 [16&preset=1\\_TRUE\\_COLOR&datasource=Sentinel-2%20L2A](https://apps.sentinel-hub.com/eo-browser/?lat=40.2685&lng=-95.6738&zoom=10&time=2019-03-16&preset=1_TRUE_COLOR&datasource=Sentinel-2%20L2A). The upper red dot in (a)  
374 represents the approximate location of the river gauge (Fig. 2c) in Turin, Iowa and the  
375 lower red dot in (a) represents the approximate location of the river gauge (Fig. 2d) in  
376 Nebraska City, NE.

377

378 Figure 2: United States Geological Survey (USGS) United States real-time streamflow for  
379 (a) November 12<sup>th</sup> 2019 and (b) March 16<sup>th</sup> 2019. The streamflow measurements are in  
380 percentiles based on the entire record of each station. Stations with under 30 years of  
381 coverage are not used. USGS gauge height (in feet) readings on the (c) Little Sioux River  
382 near Turin, IA and (d) Missouri River near Nebraska City from 1 November 2018 to 31  
383 March 2019. USGS gauge data available at <https://waterdata.usgs.gov/nwis/rt>. Panel (e)  
384 are the Climate Prediction Center Leaky Bucket Model modeled soil moisture percentiles  
385 for January 2019.

386

387 Figure 3: National Oceanic and Atmospheric Association Optimum Interpolation Sea  
388 Surface Temperature (SST) V2 anomalies for (a) September, October and November 2018

389 and (b) December 2018, January, and February 2019 in °C. Anomalies were calculated  
390 using the 1981-2010 base period climatology.

391

392 Figure 4: Global Historical Climatology Network (GHCN) station (a) monthly surface  
393 daily temperature anomalies for December and January °C, (b) monthly surface daily  
394 average temperature anomalies for February and March 2019 in °C, (c) monthly  
395 precipitation percent of normal for December 2018 and January 2019, (d) monthly  
396 precipitation percent of normal for February and March 2019. Stations were filtered by  
397 length of record, with only stations having at least 50 years of data prior to 2019 being  
398 accepted into the analysis. Anomalies were calculated using the period of record for each  
399 station. Daily temperature averages were computed as an average between the maximum  
400 and minimum daily temperature averages for each month. Station 2018-2019 snow season  
401 snowfall total records include a red symbol, with a circle representing a new record, a star  
402 is for a 2<sup>nd</sup> highest snowfall observation, 3 lines for a 3<sup>rd</sup> highest snowfall observation, 2  
403 lines for a 4<sup>th</sup> highest snowfall observation, and a triangle for a 5<sup>th</sup> highest snowfall  
404 observation.

405

406 Figure 5: (a) Automated Weather Data Network (AWDN) 7-day soil temperature (°C)  
407 observations for 6 March to 12 March. National Operational Hydrologic Remote Sensing  
408 Center (NOHRSC) modeled (b) snow depth in cm for 9 March 2019 (c) 15 March and (d)  
409 snow water equivalent in cm for 9 March 2019 and (e) 15 March. Available at  
410 <https://www.nohrsc.noaa.gov/>.

411

412 Figure 6: NCEP/NCAR Reanalysis daily averaged data for 12 March. Panel (a) is the daily  
413 averaged 500 sea level pressure (contoured) and the standardized anomaly (color filled) for  
414 March 12<sup>th</sup>. Geopotential height contours go from 900 to 1050 by 10 mb and the  
415 standardized anomalies are color filled from -8 to 8 by 1. Panel (b) is the daily averaged  
416 500 sea level pressure (contoured) for March 13<sup>th</sup>. The contours for (b) are the same as (a).  
417 Panel (c) is the daily averaged 500 hPa geopotential height (contoured) and the  
418 standardized anomaly (color filled) for March 12<sup>th</sup>. Geopotential height contours from 5300  
419 to 5700 with 60 m interval and the standardized anomalies are color filled from -6 to 6 by  
420 1. Panel (d) is the daily averaged 500 hPa geopotential height (contoured) and the  
421 standardized anomaly (color filled) for March 13<sup>th</sup>. The contours for (d) are the same as  
422 (c).

423

424 Figure 7: NCEP/NCAR Reanalysis (a) 925 mb  $v$  wind standardized anomalies. Panel (b)  
425 are the reanalysis 925 moisture advection standardized anomalies ( $\text{g kg}^{-1} \text{s}^{-1}$ ), specific  
426 humidity standardized anomalies ( $\text{g kg}^{-1}$  contoured from -12 to 12 by 2) and standardized  
427 anomaly vector wind. Panel (c) is the surface (1000 hPa) temperature standardized  
428 anomalies ( $^{\circ}\text{C}$ ). Panel (d) is the precipitable water standardized anomalies ( $\text{kg m}^{-2}$ ).  
429 Anomalies are from the two-day period of 12 March through 13 March 2019.

430

431 Figure 8: WPC QPF forecast made on 11 March for the 72-hour period beginning on 12  
432 March at 0000 UTC and ending on 15 March at 0000 UTC.

433

434 Figure 9: Panel (a) Composite radar mosaic for March 13<sup>th</sup> 2019 at 0855 UTC from the  
435 UCAR Warm Season Precipitation Episodes image archive available at  
436 <http://www2.mmm.ucar.edu/imagearchive/>. Panel (b) Composite radar mosaic for March  
437 13<sup>th</sup> 2019 at 1555 UTC from the UCAR Warm Season Precipitation Episodes image  
438 archive. Panel (c) CPC Global Unified Gauge-based daily precipitation analysis for 12-14  
439 March. Precipitation is in mm. Panel (d) is the accumulated snow for 12-15 March 2019 in  
440 inches. Available at <https://www.weather.gov/fsd/20190314-Flooding>.

441  
442  
443  
444  
445  
446  
447  
448  
449  
450  
451  
452  
453  
454  
455  
456  
457  
458  
459  
460  
461

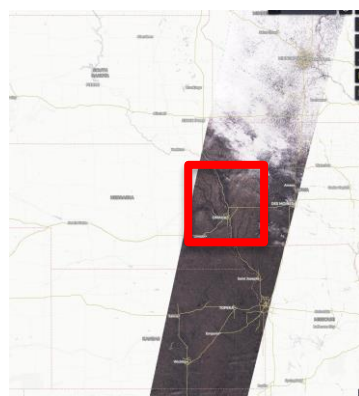
462

## Figures

463

464

(a)



(b)

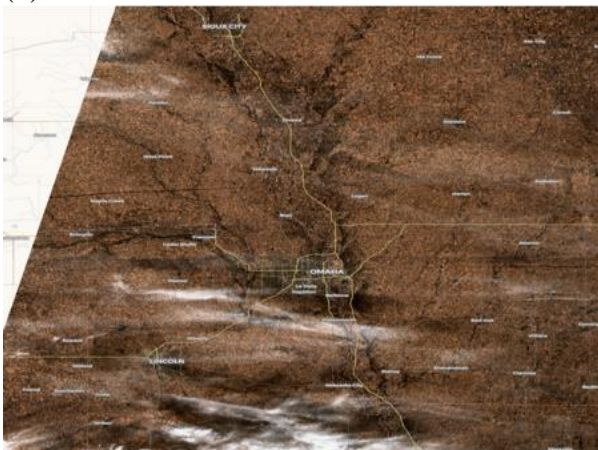


Figure 1: European Space Agency (ESA) (a) Sentinel-2A Level-1C visible band satellite image on 16 March 2019. Panel (b) Sentinel-2A Level-1C visible band satellite image on 10 January 2019. Also included is a zoomed-out image from 16 March 2019 showing the location of the zoomed in area for (a) and (b). Sentinel-2 images taken from [https://apps.sentinel-hub.com/eo-browser/?lat=40.2685&lng=-95.6738&zoom=10&time=2019-03-16&preset=1\\_TRUE\\_COLOR&datasource=Sentinel-2%20L2A](https://apps.sentinel-hub.com/eo-browser/?lat=40.2685&lng=-95.6738&zoom=10&time=2019-03-16&preset=1_TRUE_COLOR&datasource=Sentinel-2%20L2A). The upper red dot in (a) represents the approximate location of the river gauge (Fig. 2c) in Turin, Iowa and the lower red dot in (a) represents the approximate location of the river gauge (Fig. 2d) in Nebraska City, NE.

465



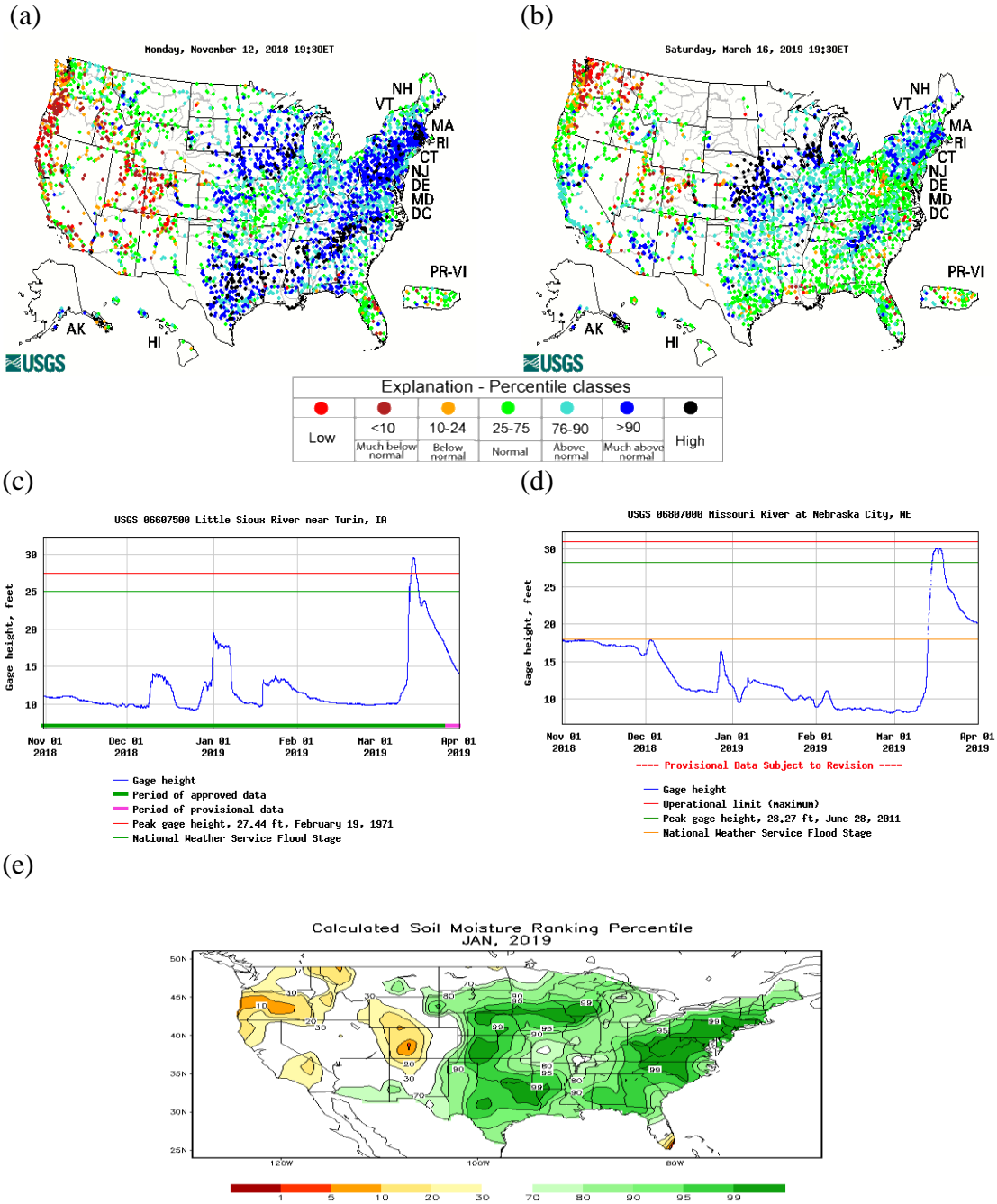


Figure 2: United States Geological Survey (USGS) United States real-time streamflow for (a) November 12<sup>th</sup> 2019 and (b) March 16<sup>th</sup> 2019. The streamflow measurements are in percentiles based on the entire record of each station. Stations with under 30 years of coverage are not used. USGS gauge height (in feet) readings on the (c) Little Sioux River near Turin, IA and (d) Missouri River near Nebraska City from 1 November 2018 to 31 March 2019. USGS gauge data available at <https://waterdata.usgs.gov/nwis/rt>. Panel (e) are the Climate Prediction Center Leaky Bucket Model modeled soil moisture percentiles for January 2019.

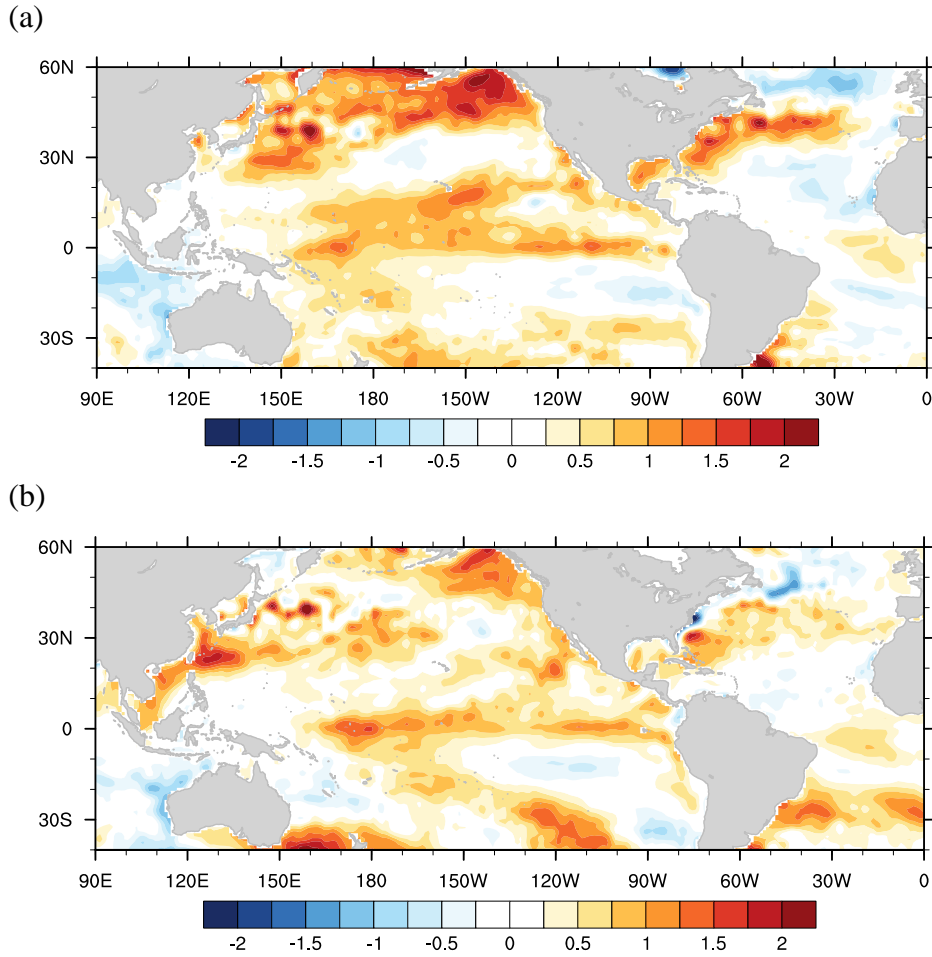


Figure 3: National Oceanic and Atmospheric Association Optimum Interpolation Sea Surface Temperature (SST) V2 anomalies for (a) September, October and November 2018 and (b) December 2018, January, and February 2019 in  $^{\circ}\text{C}$ . Anomalies were calculated using the 1981-2010 base period climatology.

467

468

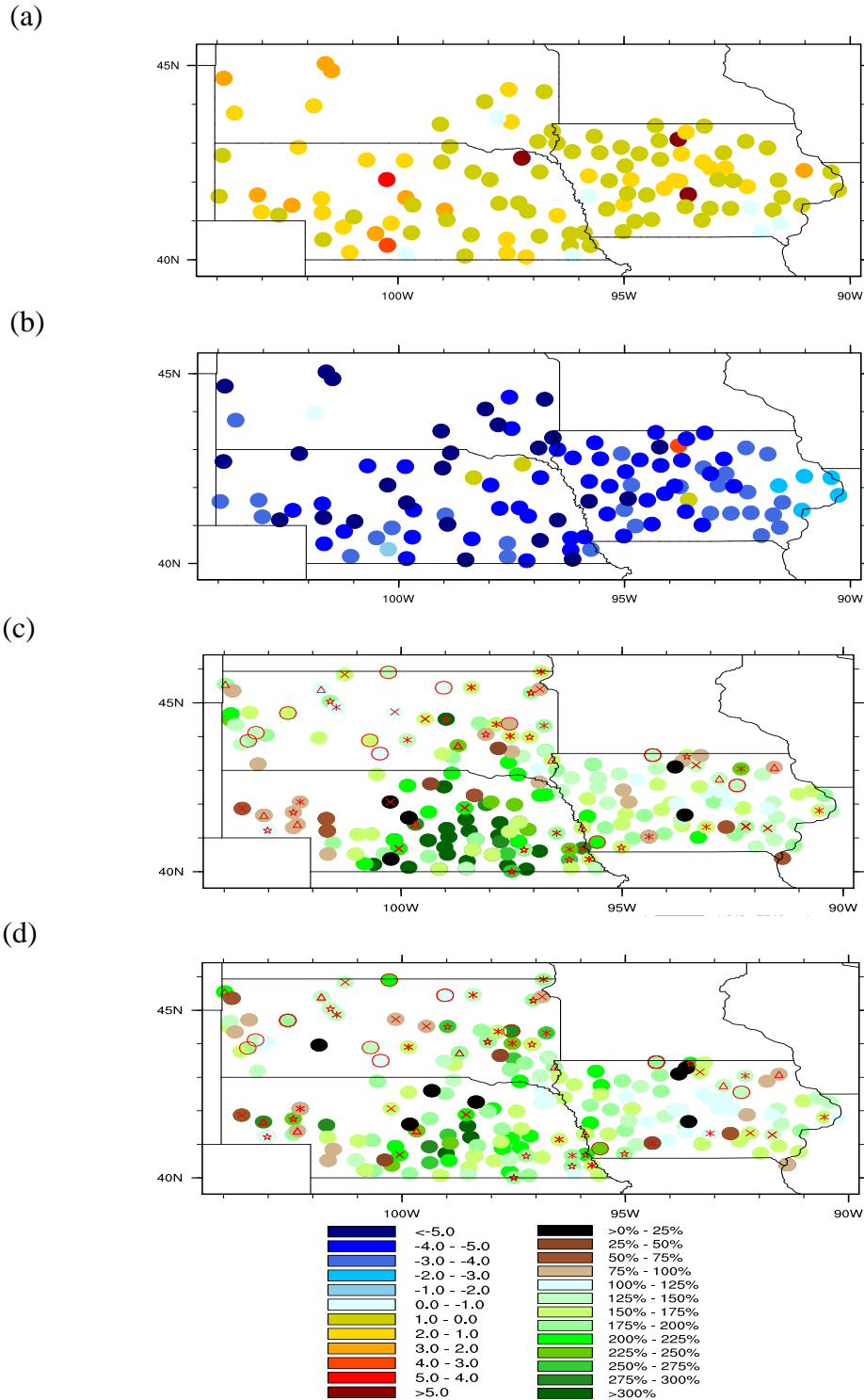


Figure 4: Global Historical Climatology Network (GHCN) station (a) monthly surface daily temperature anomalies for December and January °C, (b) monthly surface daily average temperature anomalies for February and March 2019 in °C, (c) monthly precipitation percent of normal for December 2018 and January 2019, (d) monthly precipitation percent of normal for February and March 2019. Stations were filtered by length of record, with only stations having at least 50 years of data prior to 2019

being accepted into the analysis. Anomalies were calculated using the period of record for each station. Daily temperature averages were computed as an average between the maximum and minimum daily temperature averages for each month. Station 2018-2019 snow season snowfall total records include a red symbol, with a circle representing a new record, a star is for a 2<sup>nd</sup> highest snowfall observation, 3 lines for a 3<sup>rd</sup> highest snowfall observation, 2 lines for a 4<sup>th</sup> highest snowfall observation, and a triangle for a 5<sup>th</sup> highest snowfall observation.

469

470

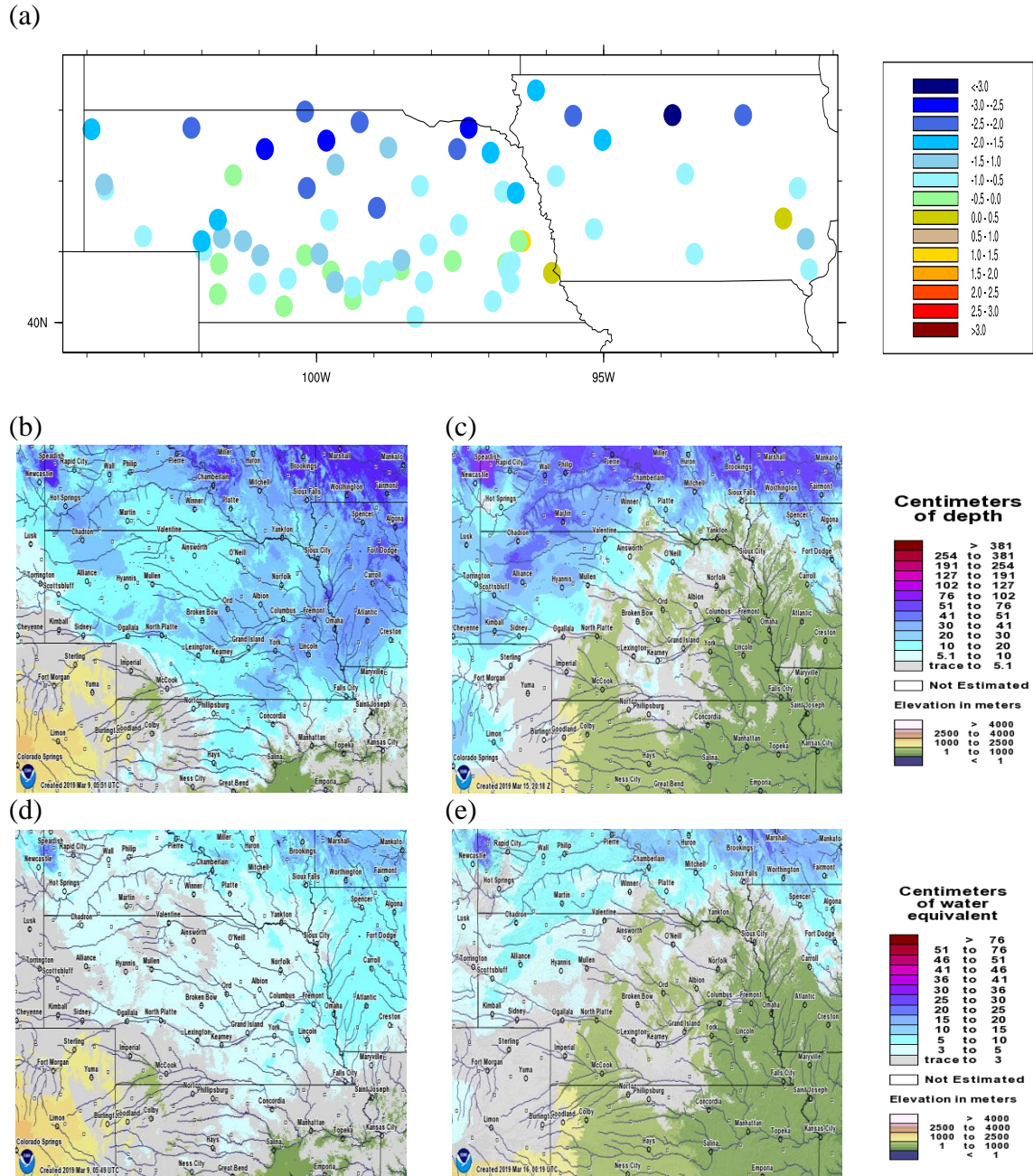


Figure 5: (a) Automated Weather Data Network (AWDN) 7-day soil temperature ( $^{\circ}\text{C}$ ) observations for 6 March to 12 March. National Operational Hydrologic Remote Sensing Center (NOHRSC) modeled (b) snow depth in cm for 9 March 2019 (c) 15 March and (d) snow water equivalent in cm for 9 March 2019 and (e) 15 March. Available at <https://www.nohrsc.noaa.gov/>.

471

472

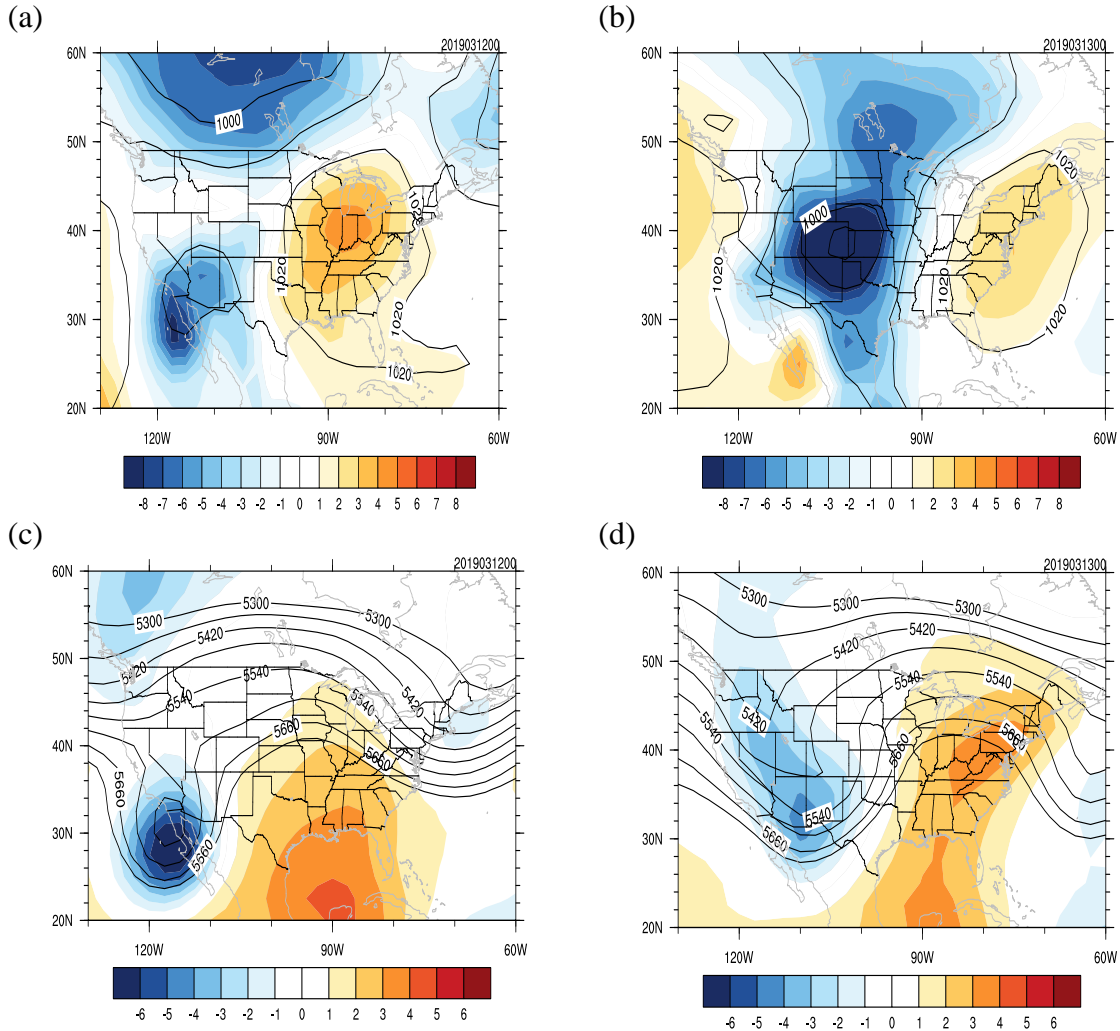


Figure 6: NCEP/NCAR Reanalysis daily averaged data for 12 March. Panel (a) is the daily averaged 500 sea level pressure (contoured) and the standardized anomaly (color filled) for March 12<sup>th</sup>. Geopotential height contours go from 900 to 1050 by 10 mb and the standardized anomalies are color filled from -8 to 8 by 1. Panel (b) is the daily averaged 500 sea level pressure (contoured) for March 13<sup>th</sup>. The contours for (b) are the same as (a). Panel (c) is the daily averaged 500 hPa geopotential height (contoured) and the standardized anomaly (color filled) for March 12<sup>th</sup>. Geopotential height contours from 5300 to 5700 with 60 m interval and the standardized anomalies are color filled from -6 to 6 by 1. Panel (d) is the daily averaged 500 hPa geopotential height (contoured) and the standardized anomaly (color filled) for March 13<sup>th</sup>. The contours for (d) are the same as (c).

473

474

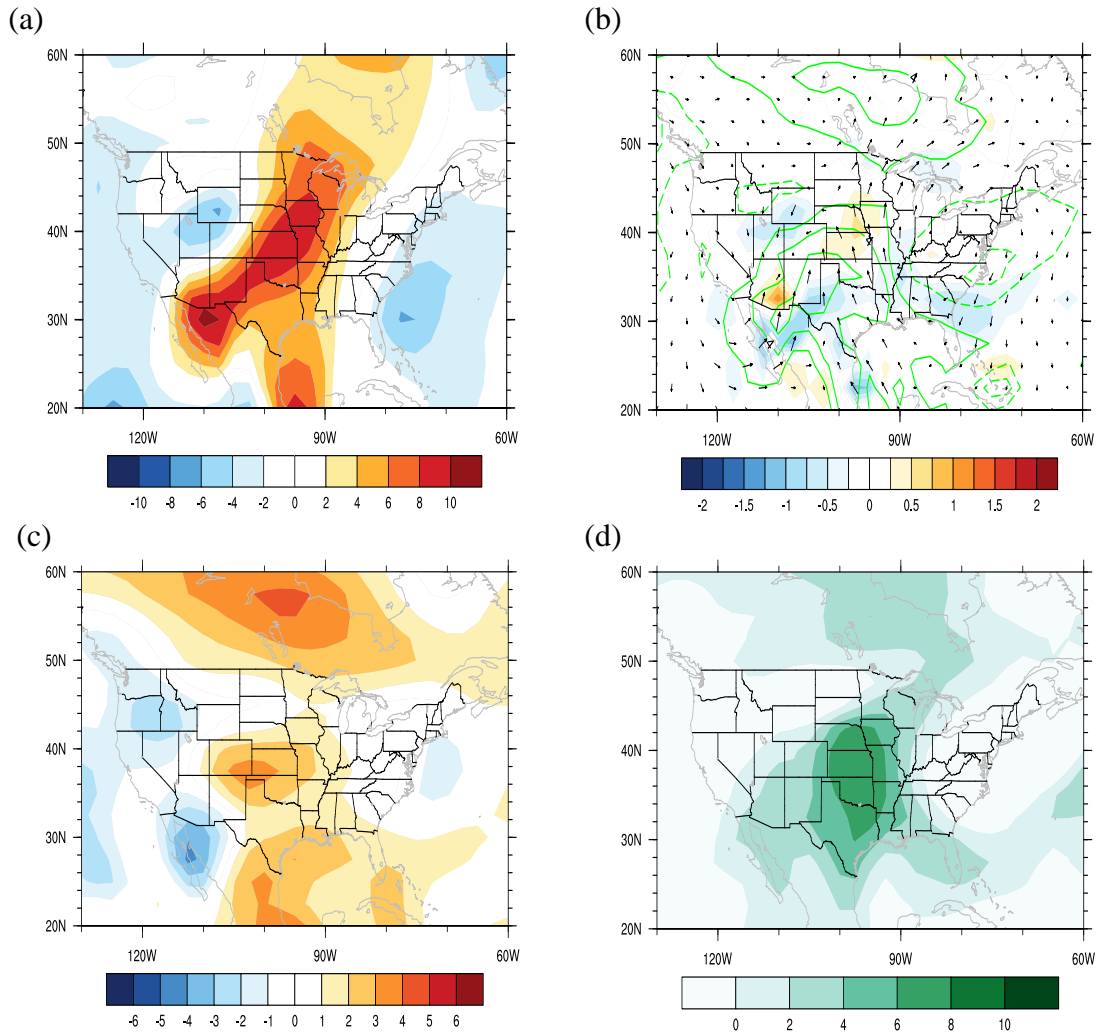


Figure 7: NCEP/NCAR Reanalysis (a) 925 mb  $v$  wind standardized anomalies. Panel (b) are the reanalysis 925 moisture advection standardized anomalies ( $\text{g kg}^{-1} \text{s}^{-1}$ ), specific humidity standardized anomalies ( $\text{g kg}^{-1}$  contoured from -12 to 12 by 2) and standardized anomaly vector wind. Panel (c) is the surface (1000 hPa) temperature standardized anomalies ( $^{\circ}\text{C}$ ). Panel (d) is the precipitable water standardized anomalies ( $\text{kg m}^{-2}$ ). Anomalies are from the two-day period of 12 March through 13 March 2019.

475

476

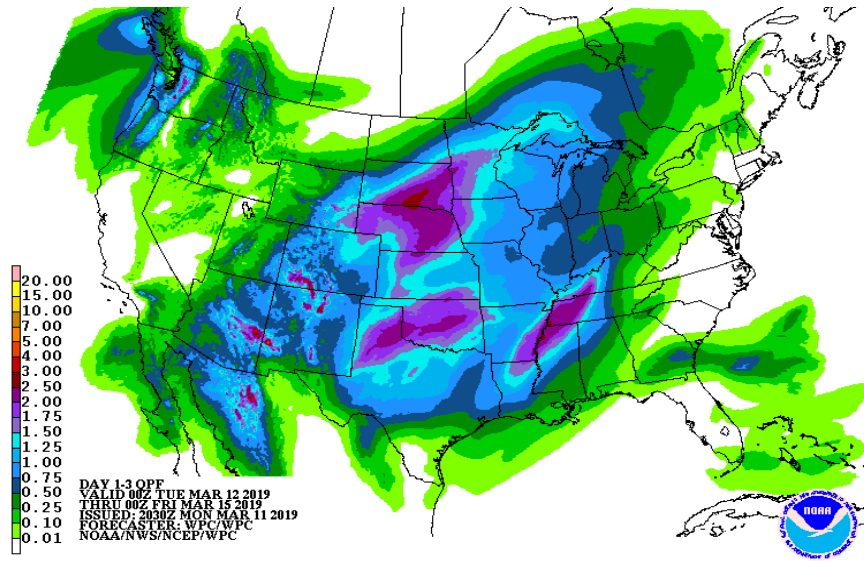


Figure 8: WPC QPF forecast made on 11 March for the 72-hour period beginning on 12 March at 0000 UTC and ending on 15 March at 0000 UTC.

477

478



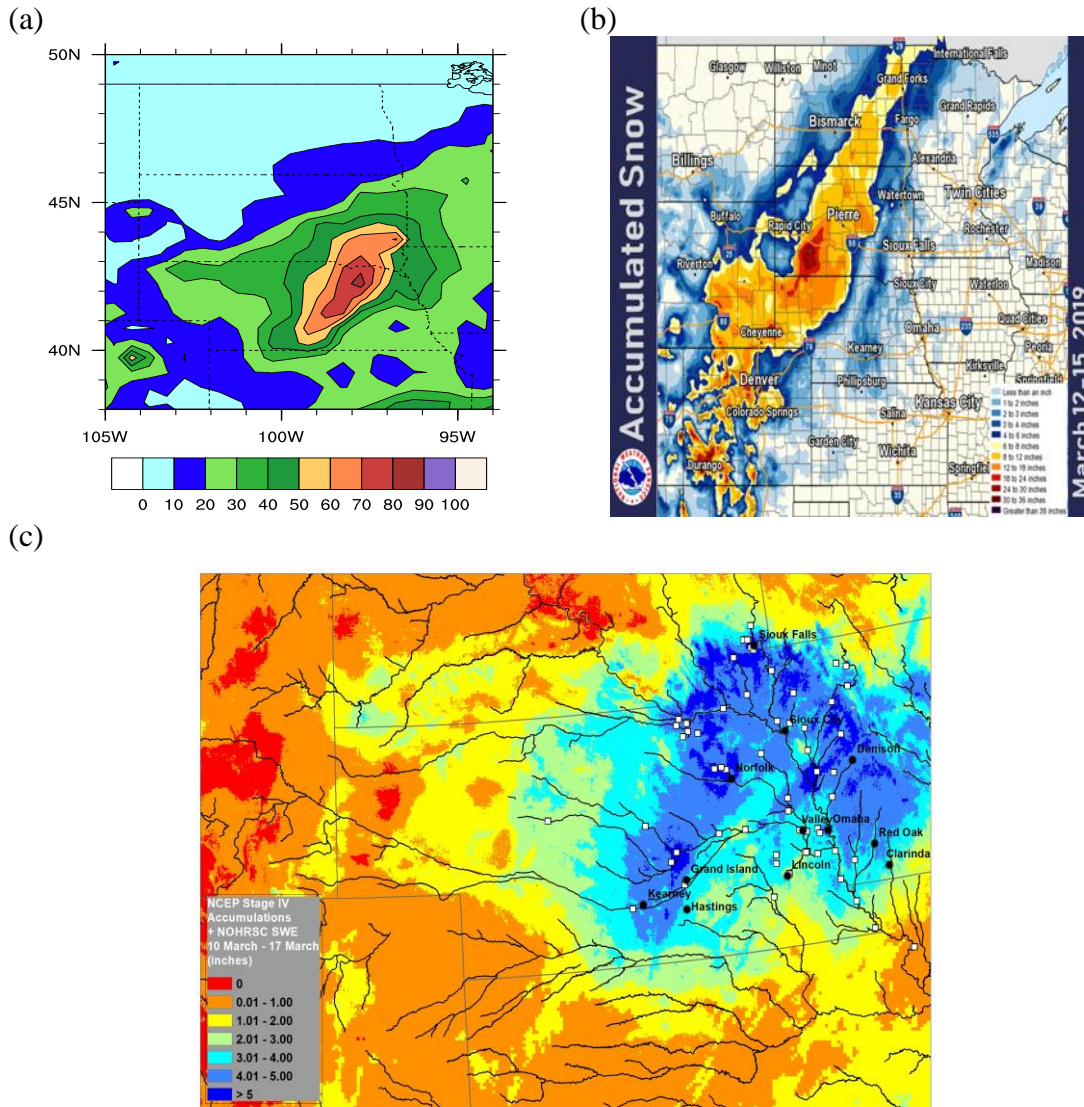


Figure 9: Panel (a) CPC Global Unified Gauge-based daily precipitation analysis for 12-14 March. Precipitation is in mm. Panel (b) is the accumulated snow for 12-15 March 2019 in inches. Available at <https://www.weather.gov/fsd/20190314-Flooding>. Panel (c) is the liquid precipitation and snow water equivalent totals for 10 March to 17 March 2019. The liquid precipitation totals are from the NCEP Stage IV product and the snow water equivalents are from the NOHRSC database. The white squares in (c) represent river gauges that set near flood stage records during the March flood event.

479

480